International Symposium
On Turbulence and Shear Flow
Phenomena (TSFP-9)
June 30 - July 3, 2015 *Melbourne, Australia*

PIV OF A PRECESSING CYLINDER FLOW AT LARGE TILT ANGLES

Thomas Albrecht, Hugh Blackburn
Department of Mechanical and Aerospace Engineering
Monash University
VIC 3800, Australia
{thomas.albrecht,hugh.blackburn}@monash.edu

Patrice Meunier
IRPHE, CNRS, and Aix–Marseille Université
49 Rue Joliot-Curie, 13013 Marseille, France
meunier@irphe.univ-mrs.fr

Richard Manasseh
Dep. of Mechanical and Product Design Engineering
Swinburne University of Technology
VIC 3122, Australia
rmanasseh@swin.edu.au

Juan Lopez
School of Mathmatical and Statistical Sciences
Arizona State University
Tempe, AZ 85287, USA
jmlopez@asu.edu

ABSTRACT

Planar particle image velocimetry measurements of the flow in a precessing cylinder are presented for nutation angles of up to 15°. For a case of a moderate Reynolds number, we observe a rapid transition to a disordered state with a brief appearance of structures of high azimuthal wave numbers. Similarity to observations reported in previous experiments and numerical simulations at much lower tilt angle, but higher Poincaré number suggests, a triadic resonance as the transition mechanism. Amplitudes of the forced mode and the mean streaming flow are extracted; their scaling with Reynolds number is found to agree reasonably well with weakly nonlinear theory.

INTRODUCTION AND BACKGROUND

Rotating flows are present in the atmosphere, in oceans and lakes, and also in astrophysical and many technical applications. A rotating system allows for inertial waves to exist owing to the restoring effect of the Coriolis force. One way to excite inertial waves is precession, the simultaneous rotation around two axes as sketched in Figure 1: a cylinder, tilted through an angle α and rotating at an angular frequency Ω_1, is mounted on a turntable which rotates at Ω_2. Precession is considered as a possible driver for the geo-dynamo, i.e., the creation of Earth's magnetic field. Also, liquid fuel in spin-stabilised spacecraft may be subject to precessional forcing, destabilising the whole spacecraft (Manasseh, 1993).

Some types of instability and transition of rotating flows may be associated with Kelvin modes, the linear, inviscid eigenmodes of solid-body rotation flow. These modes are not solutions of the full Navier-Stokes equations with no-slip boundary conditions. Yet in the weakly nonlinear regime they have proven to be useful diagnostics of experimental and numerical observations (Meunier *et al.*, 2008; Blackburn *et al.*, 2014). Each Kelvin mode is characterised by three integer indices (n,l,m) corresponding to axial, radial, and azimuthal directions, respectively, and is associated with a frequency. Velocity components of Kelvin modes all have radial profiles $u_i(r)$, $v_i(r)$, $w_i(r)$ consisting

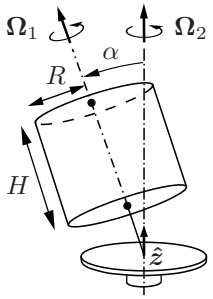

Figure 1. Schematic of precessional forcing: a cylinder, tilted through a nutation angle α and rotating at Ω_1, is mounted on a turntable which rotates at Ω_2.

of Bessel functions, and a sinusoidal axial and azimuthal structure. Figure 2 shows the four lowest-order modes. Further details are given e.g. in Meunier *et al.* (2008).

There are an infinite number of Kelvin modes. Precessional forcing can excite Kelvin modes with $m = 1$ in the case of a cylinder (or $m = 2$ for ellipsoids). If (1) a Kelvin mode's frequency matches the forcing frequency and (2) that mode's axial wave length fits the container's height H (i.e., $n\pi/k = H, n = 1,2, \ldots$), the mode is resonant. Resonant modes can grow to a large amplitude limited by viscosity or non-linearity. A mode forced outside of a resonance will still grow, but that growth is additionally damped depending on the amount of detuning. For resonant conditions and at large enough Reynolds numbers, a Kelvin mode may become unstable. This opens one possible route to turbulence in rotating flows.

Johnson (1967), Malkus (1968) and Manasseh (1992) observed a rapid transition from laminar to turbulent flow called catastrophic collapse. This transition may be explained by several competing theories: instability of a single Kelvin mode as outlined above, nonlinear interaction of three Kelvin modes known as triadic resonance, boundary layer instability, or modification of the base flow by mean streaming flow (Kobine, 1996) possibly leading to centrifugal instability.

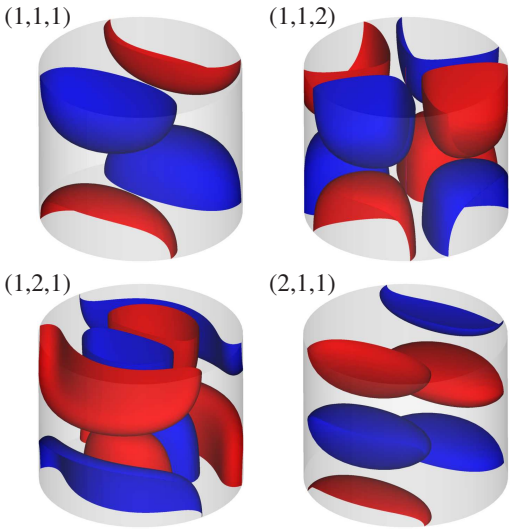

Figure 2. Iso-surfaces of axial vorticity showing the theoretical shape of the lowest order Kelvin modes.

Experimental evidence of triadic resonance in a precessing flow at a small tilt angle $\alpha = 1^\circ$ was presented by Lagrange *et al.* (2008). They used a cylinder of aspect ratio $\Gamma = H/R = 1.62$ at a Reynolds number $\mathrm{Re} = \Omega_1 R^2/\nu = 7670$ and a Poincaré number $\mathrm{Po} = \Omega_2/\Omega_1 = -0.15$, where R is the radius of the cylinder, and ν the kinetic viscosity. When forcing (denoted by an index F) the $m_F = 1$ mode, PIV visualisations clearly showed two parasitic modes $m_1 = 5$ and $m_2 = 6$, satisfying the triadic resonance condition $m_F = |\pm m_1 \pm m_2|$. Equivalent conditions exist for the modes' frequencies and their axial wavenumbers. Theory developed in Lagrange *et al.* (2011) revealed that an aspect ratio of 1.62 in fact enables the most unstable, exact resonant triad.

This case was studied numerically in Blackburn *et al.* (2014) and may serve here to demonstrate the dynamics of the flow. Reproduced in Figure 3 is the history of kinetic energy of azimuthal Fourier modes in the cylinder frame of reference (in which the kinetic energy in $m = 0$ contains no contribution of solid body rotation). Three distinct stages are clearly visible: (1) an initial, seemingly steady state where the forced mode's energy is saturated and higher azimuthal modes are slaved to the $m = 1$ mode, followed by (2) an instability where triad interaction feeds energy from mode 1 to modes 5 and 6; while this is likely to have started with the initial saturation of mode 1, it does not become apparent before $t = 130$ (where $t = t^*/T$ is the nondimensional time based on the cylinder rotation period). In the late stage of this instability, higher modes grow to large amplitudes, possibly saturated by an increasing $m = 0$ mode and a decrease in $m = 1$, finally leading to (3), an asymptotic state where higher modes retain high energy levels or enter limit cycle oscillations.

Existence of triadic resonances has recently been questioned for the case of a cylinder of $\Gamma \approx 2$ and a large tilt angle of 45° (Kong *et al.*, 2015). Accurate PIV measurements in Lagrange *et al.* (2008) and Meunier *et al.* (2008) were limited to small tilt angles, largely due to practical restrictions of their experimental setup. We will extend their work using a significantly improved setup: with the recent commissioning of a large rotating platform we can now mount the complete PIV system (laser, camera, computer) along

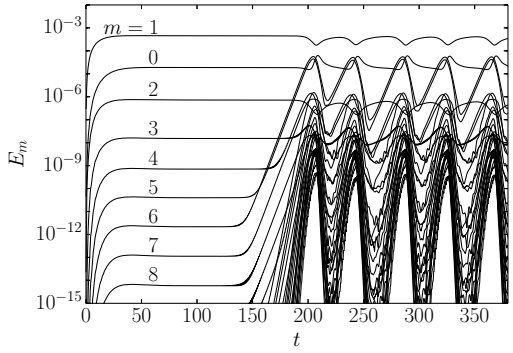

Figure 3. History of Fourier modal kinetic energy for the DNS of Blackburn *et al.* (2014), in the gimbal frame of reference. $\Gamma = 1.62$, $\mathrm{Re} = 7670$, $\mathrm{Po} = -0.15$, $\alpha = 1^\circ$.

with the precessing cylinder in the rotating table frame. This allows us to tilt the laser light sheet with the cylinder. Larger tilt angles of up to 15° are now possible; previously this would have resulted in significant errors.

We report new results from PIV measurements at an aspect ratio of 1.835, tilt angles up to 15° and Reynolds numbers ranging from 6×10^3 to 10^5. In all our experiments, the first Kelvin mode is forced at its first resonance. Saturation amplitudes of Kelvin modes are extracted and compared to scaling laws suggested in Meunier *et al.* (2008). For a weakly forced case (large tilt angle, but small Poincaré number), we observe dynamics similar to Blackburn *et al.* (2014), suggesting a triadic resonance.

We then focus on quantifying the mean streaming flow. While inviscid Kelvin modes generate no mean streaming flow (an axisymmetric flow), streaming occurs as a consequence of viscous modification of Kelvin modes at finite Reynolds numbers, i.e. boundary layer structure, and nonlinear terms in the equations of motion. Characterising the mean streaming flow is important because it changes the base flow away from solid-body rotation, therefore breaking the underlying assumption; also it detunes the resonances of the Kelvin modes. It directly impacts all of the proposed transition mechanisms. So far, no theory has succeeded in predicting the amplitude or spatial structure of the mean streaming flow. Finally, our data will allow validation of accompanying direct numerical simulations.

EXPERIMENTAL SETUP

Figure 4 shows our experimental setup. A cylinder, filled with water and spinning at Ω_1, is mounted on a DC motor's axis. A rotary encoder measures the motor's angular velocity with an accuracy of 0.1%. The cylinder is made from Perspex and has an inner radius $R = 46.2\,\mathrm{mm} \pm 0.1\,\mathrm{mm}$. Its effective height H can be varied by using different insets. Aligned with the axis and facing the cylinder's top, a Redlake ES 11000 11 megapixel camera records PIV images. Motor, cylinder and camera are mounted on a gimbal which can be tilted to an angle α of up to 15° by a linear stepper motor. The accuracy of the tilt angle is 0.1°. A light sheet created by a 250mJ dual-pulse NdYAG laser (Big Sky Laser) and cylindrical lenses illuminates a cross-section of the tilted cylinder at a height $z_{PIV} = z/H$. The coordinate system is fixed at the centre of the cylinder. Together with a PC controlling the camera, all of the above is

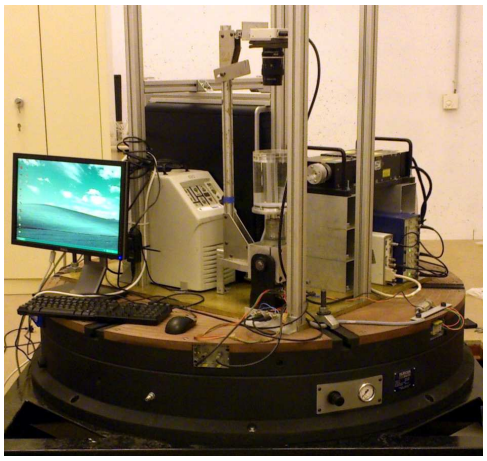

Figure 4. Experimental setup: water-filled cylinder, PIV camera and laser, and computer mounted on a rotating table.

mounted on a large platform rotating at Ω_2. The total rotation along the axis of the cylinder in the inertial frame of reference is $\Omega = \Omega_1 + \Omega_2 \cos\alpha$. Initially, the cylinder was spinning upright to establish a solid body rotation. It was then tilted (defining $t = 0$) and 200 image pairs (the maximum permitted by available memory) of the transient flow were recorded at 1 Hz. Once the images were written to the hard disk—about 6 minutes after the tilt—the flow was assumed to have reached an asymptotic state and another 50 image pairs were recorded.

PIV PROCEDURE, VALIDATION, AND POST-PROCESSING

Since the camera is mounted in the gimbal frame of reference, it mainly records solid-body rotation flow. To recover the secondary flow we remove the cylinder rotation by counter-rotating the image pairs prior to the PIV cross-correlation. Here, it is essential to know the exact centre of rotation in image coordinates since errors in its position $\Delta\mathbf{x}_c$ introduce a spurious mean velocity $\sim \Delta\mathbf{x}_c/\Delta t$, where Δt is the time separation of an image pair. However, we found the centre of rotation in image coordinates could differ between experiments (when the cylinder had been removed and re-placed) or even move during one experiment (when the tilt occurred, the cause of which remained unclear). We therefore had to adopt a mostly automatic procedure to obtain the centre of rotation for each experiment individually: (1) iteratively identify the cylinder wall at eight azimuthal locations by finding radial step changes of image brightness averaged over segments of 15°, (2) fit an ellipse to the eight wall locations, and (3) time-average the centre to eliminate wobbling due to a slight misalignment of camera axis and cylinder axis.

Figure 5 compares PIV results to a direct numerical simulation (DNS) using a spectral-element Fourier method (Blackburn & Sherwin, 2004) to validate both approaches. Details of the numerical setup in the rotating frame of reference are given in Blackburn *et al.* (2014). Reynolds number and tilt angle were chosen such that the forced mode is still dominant. Symbols show the in-plane velocity components extracted along a diameter from time-averaged PIV data. Lines show an equivalent extraction from DNS. For $\alpha = 15°$ and $\mathrm{Re} = 558$ (Figure 5a) we find an almost perfect agreement for both velocity components. At a smaller

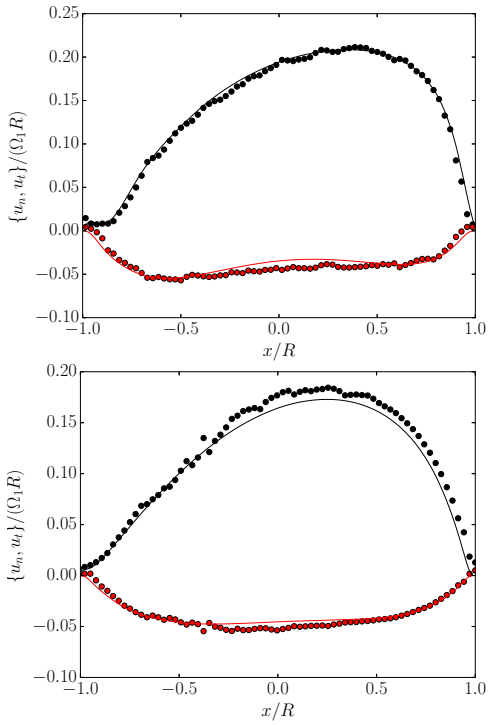

Figure 5. Time-averaged velocity components normal (black) and tangential (red) to the direction of tilt, extracted along a diameter in a plane at one quarter of the cylinder height, from PIV (symbols) and DNS (lines). $\Gamma = 0.457$, $\mathrm{Po} \approx -0.475$. (a), $\alpha = 15°$ and $\mathrm{Re} = 558$; (b), $\alpha = 5°$ and $\mathrm{Re} = 1440$.

angle $\alpha = 5°$, but higher $\mathrm{Re} = 1440$, the PIV velocities are slightly larger than the numerical predictions, perhaps caused by a small absolute error in the tilt angle, which becomes more severe at smaller angles. Still, the agreement is very good, and we conclude our PIV measurements are reliable.

The measured radial and azimuthal velocity components u, v were projected onto an equivalent slice of the Kelvin mode's velocity u_i, v_i as described in Meunier *et al.* (2008). (For brevity, the set of integers (n,l,m) is denoted i where the exact integers are irrelevant.) We assume the experimental in-plane velocity at height z is

$$\begin{pmatrix} u \\ v \end{pmatrix} = \Omega R \mathrm{Ro} \sum_i a_i \sin(k_i z) \begin{pmatrix} -i\sin(\varphi+\beta_i)u_i(r) \\ \cos(\varphi+\beta_i)v_i(r) \end{pmatrix}, \quad (1)$$

i.e., consists of a sum of Kelvin modes, each rotated by angle β_i. Exploiting the orthogonality of the Kelvin modes, one can obtain the non-dimensional amplitude a_i. Note that the effect of forcing amplitude is accounted for by the Rossby number $\mathrm{Ro} = \Omega_2 \sin\alpha/\Omega$ in Eq. (1); in the linear regime, a change in tilt angle should not affect a_i, everything else being constant. Yet we will mostly present dimensional amplitudes $\Omega R \mathrm{Ro} a_i$ in the following.

The amplitude of the mean streaming flow a_0 is difficult to quantify. No theory exists for the radial profile onto which the measured velocity could be projected. Instead, we extract the maximum $\hat{v}_0$ of the azimuthally averaged azimuthal velocity $v_0(r)$ in the gimbal frame of reference and define a_0 via $\hat{v}_0 = \Omega R \mathrm{Ro}\, a_0$.

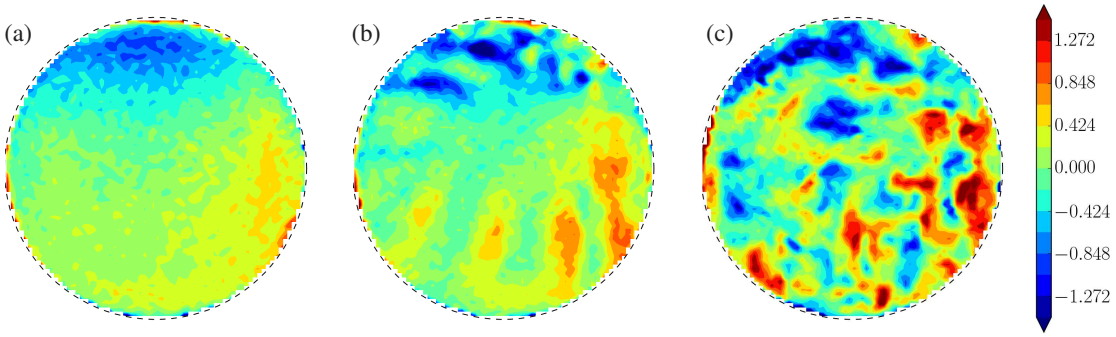

Figure 6. Instantaneous axial vorticity at one quarter of the cylinder height in $1/s$ at (a) $t = 16.5$, (b) 21.3, and (c) 24.2; $\Gamma = 1.835$, Re $= 6000$, Po $= -0.0679$, $\alpha = 15°$.

INITIAL DYNAMICS

We carried out a series of experiments varying tilt angle and Reynolds number at an aspect ratio $\Gamma = 1.835$. Forcing the first mode at its first resonance yields an approximately constant Poincaré number in the range $-0.0689 \leq$ Po ≤ -0.0666 (retrograde precession). Note that this aspect ratio does not allow for an *exact* resonant triad as studied in Lagrange *et al.* (2008); here, no two parasitic modes exist that are *exactly* resonant with the forced mode.

We first describe the dynamics following the tilt, including a rapid transition from a seemingly steady state dominated by the forced mode, to a disordered state, for an exemplary case Re $= 6000$, $\alpha = 15°$, Po $= -0.0689$. Despite the large tilt angle, we still expect weakly nonlinear behaviour because the Poincaré number is small.

Figure 7(a) shows the evolution of the first four (radial) Kelvin modes ($n = 1$, l, $m = 1$) after the tilt. The time axis is split to accommodate both the first PIV recording directly following the tilt at $t = 0$ and the second recording starting at $t \approx 200$. Kelvin mode amplitudes show similar dynamics as the Fourier mode energies observed in the DNS of Blackburn *et al.* (2014) (cf. Fig. 3). We find a steep initial rise of the forced Kelvin mode (1,1,1) which then (after an overshoot) saturates around $t = 15$ and dominates the Fourier energy of that mode—the amplitudes of the $m = 1$ Kelvin modes of higher radial wavenumber remain small at all times. Contours of instantaneous axial vorticity at $t = 16.5$, extracted from a plane at quarter-height of the cylinder and shown in Fig. 6(a), exhibit dominance of azimuthal wave number $m = 1$, accompanied by a barely visible $m = 2$ structure, and in accord with Fig. 3.

Around $t = 25$, the amplitude of the forced Kelvin (Fig. 7a) mode drops slightly, then reaches an asymptotic state by $t = 40$ which persists throughout the second measurement. A similar decrease is observed in Fig. 3 for $m = 1$ at $t \approx 200$, associated with the parasitic modes $m = 5$ and 6 growing to large amplitudes. Weakly nonlinear theory based on a triadic resonance (Lagrange *et al.*, 2011) predicts that Kelvin modes $m = 5$ and 6 are the most unstable ones for aspect ratios $1.62 \leq \Gamma \leq 3.6$, including $\Gamma = 1.835$ of the current experiment, in which higher modes first become apparent in the measured axial vorticity at $t = 17.9$. A snapshot at $t = 21.3$ in Fig. 6(b) reveals structure predominant in the bulk of the flow which appears to have even higher azimuthal wave numbers than 5 and 6, although these could be harmonics. Fourier analysis of the velocity components for $0.6 \leq R/R_{max} \leq 0.85$ showed dominance of $m = 1$ and 2, followed by roughly equal contributions of modes 5–10. Kelvin mode projections similar to Fig 7 for modes up to

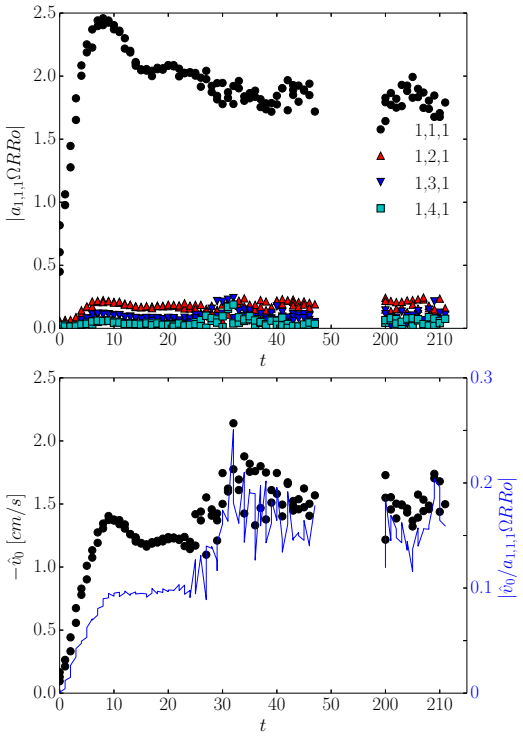

Figure 7. Amplitudes of (a) the first four radial Kelvin modes $(n = 1, l, m = 1)$, and (b) the mean streaming flow, during the first PIV recording $0 \leq t \leq 48$ following the tilt, and during the second recording $200 \leq t \leq 213$. The blue line in (b) shows the ratio of the mean streaming flow and the forced mode's amplitude.

$m = 10$ show modes $m > 2$ are absent before and appear during the instability, although the data is rather noisy owing to the limited PIV resolution.

During the instability, the vorticity structures pulsate with a frequency on the order of half the PIV image acquisition frequency ($f_{PIV} = 1$ Hz, the non-dimensional period $1/(f_{PIV}T) = 0.48$) and grow rapidly until azimuthal structure is no longer discernible at $t = 24.2$. Hence, this transition to disordered flow is observable only over a very short time of approximately six cylinder revolutions.

This transition is also very evident in the amplitude of the mean streaming flow $\hat{v}_0$ plotted in Figure 7(b). Note that the Y-axis shows the negative of the amplitude; the mean

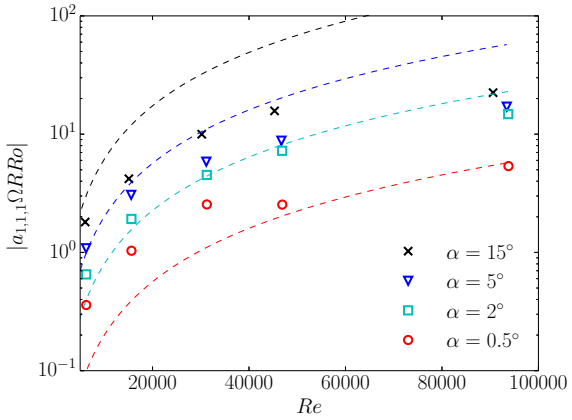

Figure 8. Dimensional amplitude of the forced Kelvin mode for various tilt angles and Reynolds numbers (symbols), and the theoretical prediction (lines). $\Gamma = 1.835$, $\mathrm{Po} \approx -0.067$.

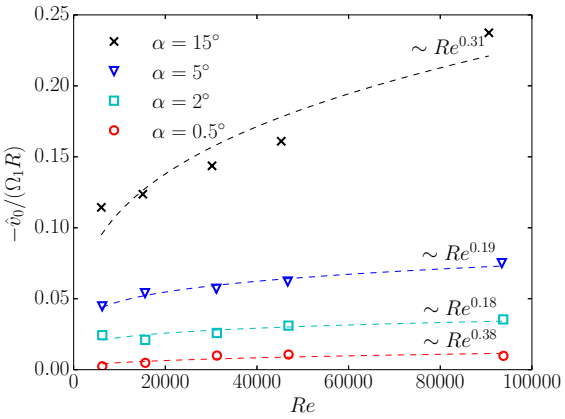

Figure 9. Amplitude of the mean streaming flow, nondimensionalised by the cylinder's circumferential velocity, for various tilt angles and Reynolds numbers (symbols). Lines show power-law fit $C\mathrm{Re}^D$. Parameters as in Fig. 8.

streaming flow decelerates the base flow. We find a similar overshoot and saturation after the tilt as for the amplitude of the force mode, and until the transition, mean streaming flow and forced mode are clearly linked as shown by their ratio plotted in blue on the alternative Y-axis. However, the mean streaming flow grows during the transition, in accord with $m = 0$ energy in Fig. 3 at $t \approx 200$.

Asymptotic state

We now report asymptotic state amplitudes of the forced Kelvin mode and the mean streaming flow, measured approximately six minutes after the tilt, for all our experiments at $\Gamma = 1.835$. The focus is on investigating the scaling with Reynolds number and tilt angle.

Kelvin mode amplitudes Symbols in Figure 8 show the measured amplitude of the forced Kelvin mode, in dimensional units. As expected, the mode amplitudes increase with Re and α. The lines show the theoretical amplitude $v_1 = |\mathrm{i}\Omega R f \mathrm{Ro}\sqrt{\mathrm{Re}}/s|$, where the complex surface viscous parameter s and the real linear forcing parameter f are given in the appendix of Lagrange *et al.* (2011). For Reynolds numbers below 5×10^4, the experimental data matches the scaling $\sim \sqrt{\mathrm{Re}}$ quite well. The linear scaling $\sim \sin\alpha$ with the tilt angle is reflected less well; the lowest angle 0.5° is constantly underpredicted by theory and the highest angles 5 and 15° are constantly overpredicted. However, the 2° data is matched very well. Note that there is no fitting parameter, the theory predicts the dimensional amplitude of the forced mode saturated by viscosity.

Mean streaming flow Figure 9 shows the amplitude of the mean streaming flow, normalised by the cylinder circumferential velocity. Note that for this aspect ratio, Ω_1 is very close to Ω. A nondimensionalisation using the total angular frequency as in Fig. 8 produces almost the same plot, yet the nondimensionalisation shown here allows to view the amplitude in relation to the base flow of solid body rotation: the largest amplitude observed is $\approx 22\%$ of the cylinder's circumferential velocity at $\alpha = 15°$ and $\mathrm{Re} = 95\,000$. As expected, the mean streaming flow increases with α. We fitted a power-law of a form $C\mathrm{Re}^D$ to the data, shown by the lines, which yields exponents D ranging from 0.18 to 0.38.

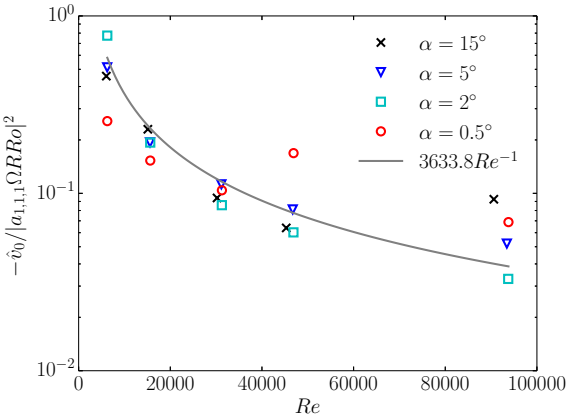

Figure 10. Amplitude of the mean streaming flow, divided by the square of the force mode's dimensional amplitude (symbols), and a fit $\sim \mathrm{Re}^{-1}$. Parameters as in Fig. 8.

Because the mean streaming flow results from nonlinear interaction of the forced mode with itself, one could expect it scales as $(a_{1,1,1})^2$. We tested this in Figure 10: this scaling indeed collapses the data for different α roughly to a single line $\sim \mathrm{Re}^{-1}$, but not to a constant.

Finally, we plotted time averaged and normalised profiles of the mean streaming flow for various tilt angles. At a given tilt angle, we find the profiles are roughly independent of Re, therefore we show data for $\mathrm{Re} \approx 46\,000$ as an example in Fig. 11. Note that all observed dimensional profiles were negative, i.e. they counteract the cylinder rotation. At low α, the profiles are generally right-skewed, although the 0.5° profile shown is a rather extreme case, perhaps affected by measurement errors due to the very low amplitude v_0. The profiles become more symmetric with increasing α.

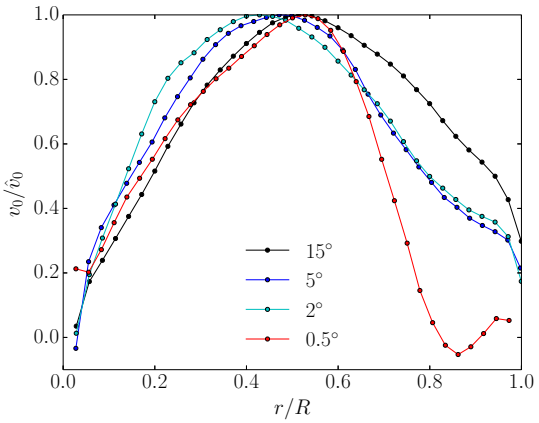

Figure 11. Profiles of the mean streaming flow normalised by their maximum value, at Re ≈ 46000, for various tilt angles. Parameters as in Fig. 8.

CONCLUSIONS

We presented planar PIV measurements of a precessing cylinder flow at a tilt angle of 15°. These experiments are the first in a series aiming to conclusively explain the resonant collapse mechanism as observed by Johnson (1967), Malkus (1968) and Manasseh (1992). For a weakly forced case which showed a rapid transition from a state dominated by the forced mode to a disordered state, structures of azimuthal wavenumber around $m \approx 8$ were observed; such wavenumbers are close to the theoretical predictions $m = 5$ and 6 based on triadic resonances (Lagrange *et al.*, 2011). Amplitudes of projections onto Kelvin modes and Fourier analysis of the velocity field suggested that multiple azimuthal modes were present. Also, these structures appeared mostly in the bulk of the flow, not close to the boundaries. Therefore, of the proposed and competing theories boundary layer instability, centrifugal instability, instability of a single Kelvin mode, and triadic resonance, the latter seems to be the most likely cause of the transition observed here.

Scalings obtained from Kelvin mode projections for the full set of experiments largely confirm theoretical predictions (Meunier *et al.*, 2008). The force mode's amplitude scales as the square root of the Reynolds number. Data for the amplitude of the mean streaming flow, defined here as the maximum of the azimuthal averaged azimuthal velocity, suggests a scaling as the square of the forced mode's amplitude, and as the inverse of the Reynolds number. Numerical simulation, feasible at Reynolds numbers up to $O(10^4)$, could further assist in finding the correct scaling.

REFERENCES

Blackburn, H. M., Albrecht, T., Mannaseh, R., Lopez, J. M. & Meunier, P. 2014 Instability in a precessing cylinder flow. In *Proc. 19th A/Asian Fluid Mech. Conf.*. Melbourne.

Blackburn, H. M. & Sherwin, S. J. 2004 Formulation of a Galerkin spectral element–Fourier method for three-dimensional incompressible flows in cylindrical geometries. *J. Comput. Phys.* **197** (2), 759–778.

Johnson, LE 1967 The precessing cylinder. Notes on the 1967 Summer Study Program in Geophysical Fluid Dynamics at the Woods Hole Oceanographic Inst. Ref. 67–54.

Kobine, J. J. 1996 Azimuthal flow associated with inertial wave resonance in a precessing cylinder. *J. Fluid Mech.* **319**, 387–406.

Kong, D., Cui, Z., Liao, X. & Zhang, K. 2015 On the transition from the laminar to disordered flow in a precessing spherical-like cylinder. *Geophys. Astrophys. Fluid Dyn.* **109**, 62–83.

Lagrange, R., Eloy, C., Nadal, F. & Meunier, P. 2008 Instability of a fluid inside a precessing cylinder. *Phys. Fluids* **20**, 081701.

Lagrange, R., Meunier, P., Nadal, F. & Eloy, C. 2011 Precessional instability of a fluid cylinder. *J. Fluid Mech.* **666**, 104–145.

Malkus, W. V. R. 1968 Precession of the Earth as the cause of geomegnetism. *Science* **160**, 259–264.

Manasseh, R. 1992 Breakdown regimes of inertia waves in a precessing cylinder. *J. Fluid Mech.* **243**, 261–296.

Manasseh, R. 1993 Visualizaton of the flows in precessing tanks with internal baffles. *AIAA J.* **31**, 312–318.

Meunier, P., Eloy, C., Lagrange, R. & Nadal, F. 2008 A rotating fluid cylinder subject to weak precession. *J. Fluid Mech.* **599**, 405–440.